2010 IEEE International Conference on Robotics and Automation
Anchorage Convention District
May 3-8, 2010, Anchorage, Alaska, USA

Design of a Multi-Disc Electromechanical Modulated Dissipator

Ryan J. Farris and Michael Goldfarb, *Members, IEEE*

Abstract— **This paper presents the design of an electrically-actuated, proportional brake that provides a significantly greater torque-to-weight ratio than a magnetic particle brake (considered a benchmark of the state-of-the-art) without sacrificing other characteristics such as dynamic range, bandwidth, or electrical power consumption. The multi-disc brake provides resistive torque through a stack of friction discs which are compressed by a dc-motor-driven ball screw. Unlike nearly all other proportional brakes, which operate in a normally unlocked mode, the brake presented here is designed such that it may be configured in either a normally unlocked or normally locked mode. The latter enables lower electrical energy consumption and added safety in the event of electrical power failure in certain applications. Following the device description, experimental data is presented to characterize the performance of the brake. The performance characteristics are subsequently compared to those of a commercially available magnetic particle brake of comparable size.**

I. Introduction

Several control applications require the use of an electrically controllable proportional rotary brake (e.g., [1]-[16]). Probably the most common and thoroughly developed example of such a device is the magnetic particle brake (MPB). Magnetic particle brakes produce a steady-state resistive torque roughly proportional to the input current. A sectioned view of a magnetic particle brake is shown in Figure 1. DC current applied to the brake coil induces a magnetic field which links fine ferrite particles to the rotating brake shaft. The amount of current in the coil determines the strength of the magnetic field, which in turn determines the resistive torque imposed on the brake shaft. Compared with the closed-loop control of a high-performance DC torque motor, these devices provide a relatively low-power and light-weight means of exerting controlled dissipative mechanical torque. Further, using an electric motor as a dissipater requires measurement of velocity, which typically contains phase lag, which in turn adds (rather than dissipates) energy to the system. A proportional brake, on the other hand, does not require velocity measurement and is guaranteed to be energetically passive.

Though the weight of a magnetic particle brake is low relative to a DC motor (for a given resistive torque), in many cases the weight remains significant. Several efforts to increase the performance of such devices have been reported, including the development of magnetorheological fluid brakes, electrorheological fluid brakes, and piezoelectrically actuated brakes (e.g., [17]-[23]). Magnetorheological and electrorheological brakes provide improved torque-to-weight characteristics relative to magnetic particle brakes, but sacrifice bandwidth and dynamic range relative to the MPB. The piezoelectrically actuated brake described in [23] offers a high bandwidth and decreases the electrical power consumption for low-frequency excitation, but provides less torque-to-weight and more torque ripple than the MPB.

This paper presents the design of an electrically-actuated proportional brake that provides a significantly improved torque-to-weight ratio relative to a magnetic particle brake, while maintaining (or improving) dynamic range and response time. Importantly, unlike particle brakes, magnetorheological fluid brakes, or electrorheological fluid brakes, the proposed device can be designed in both a normally unlocked and normally locked configuration, which offers a greater number of design options for a given application. The approach utilizes a motor-driven ball screw, which compresses a multiple-disc mechanism for resistive torque generation. Due to the amplification effects of a small ball screw lead and a large number of discs in the disc stack, the brake provides a resistive torque approximately three orders of magnitude larger than the motor torque. Due to the relatively thin discs used on the brake, the authors refer to the device as a wafer disc brake (WDB).

Note that electrically actuated multiple disc brakes and clutches are commercially available and used in heavy equipment applications (e.g., material handling). Such brakes, however, operate similarly to a magnetic particle brake, in that they utilize a stack of ferrous discs subjected to an electrically induced magnetic field. Such brakes are effective, but due to residual magnetism and sticking of plates, do not provide well-behaved proportional operation. Further, due to the nature of the attractive forces generated by a magnetic field, implementation of such brakes in a normally locked configuration would be a nontrivial task. The remainder of this paper describes the design of the (wafer disc) brake and characterizes and compares its performance to that of a commercially available magnetic particle brake of comparable size.

II. Wafer Disc Brake Design

A. Brake Configuration

The normally unlocked configuration of the WDB is shown in cross-section in Fig. 2. The normally unlocked brake consists of a stack of thin (0.25 mm) high-strength plastic wafers which are alternately coupled (through

Manuscript received September 15, 2009.

R. J. Farris is with Vanderbilt University, Nashville, TN 37235 USA (e-mail: ryan.farris@vanderbilt.edu phone: 615-343-2782; fax 615-343-6925).

M. Goldfarb is with Vanderbilt University, Nashville, TN 37235 USA (e-mail: michael.goldfarb@vanderbilt.edu).

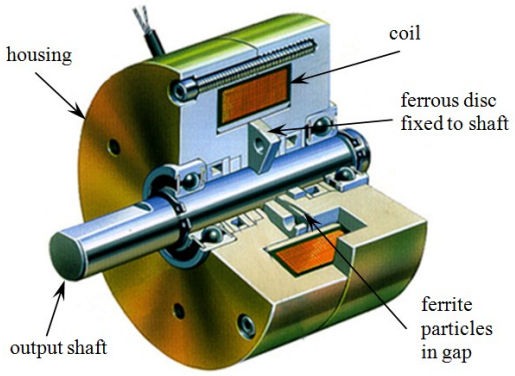

Fig 1. Sectioned view of a magnetic particle brake taken from PrecisionTork.com.

splines) to the brake stator and rotor. A small brushless motor located inside the brake stator transmits a compressive force through a ball screw to the stack. Assuming relatively low friction in the ball screw, the stack is subjected to a compressive force which is proportional to the motor current. Due to the series arrangement of discs, the resistive torque on the rotor barrel is the product of the compressive force, the mean radius of contact, and the coefficient of friction, which is amplified by the number of interfaces between discs. Since the brake (as shown) contains 45 discs, the effective torque is increased by a gain of 44. Since the ball screw is back-drivable, the brake torque remains in proportion to the motor current, and thus is proportional in nature. A compression spring is located between the motor and ball screw nut to insure full torque release when zero electrical power is supplied. Note that the brake as shown does not incorporate a central shaft, as is typical in many brakes, but rather incorporates an annular rotor "barrel." The use of an annular rotor (and the lack of a central shaft) is not fundamental to the brake design, but rather was opted for by the authors in order to better integrate the brake into a mechanism (i.e., similar to the use of a frameless motor). The WDB in its normally locked configuration is shown in cross-section in Fig. 3. The design of the normally locked brake is similar to the normally unlocked type, but the discs are preloaded with a compression spring. Applying current to the motor proportionally unloads the preload, such that full brake torque occurs at zero motor current, and minimum brake torque occurs at full motor current. Since the ball screw is back-drivable, the brake torque remains in inverse proportion to the motor current. Both configurations of the WDB appear the same from the outside. A photo of a fully functional wafer disc brake (which has been configured in both a normally locked and normally unlocked configuration) is shown in Fig. 4.

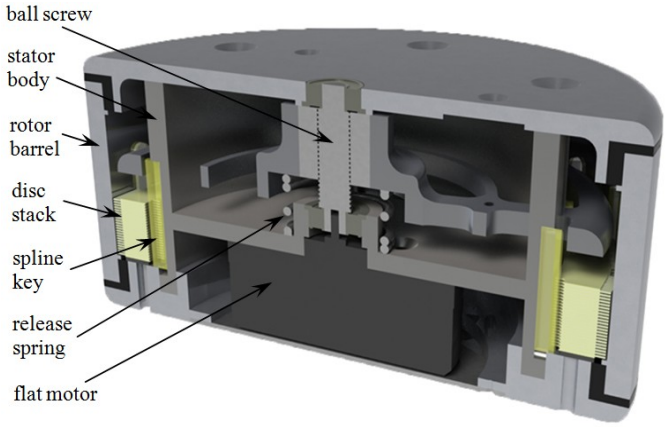

Fig. 2. Sectioned view of normally unlocked wafer disc brake.

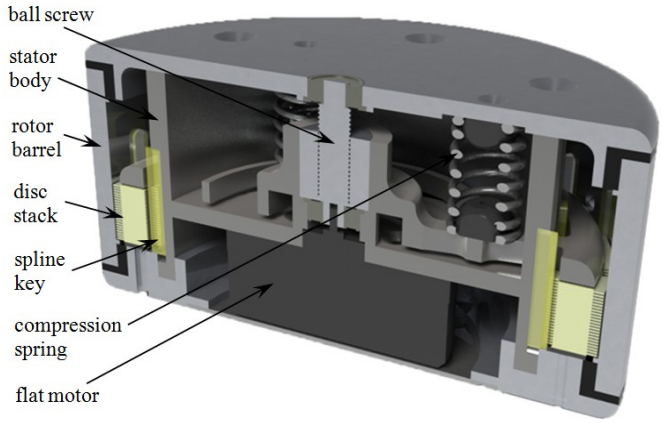

Fig. 3. Sectioned view of normally locked wafer disc brake.

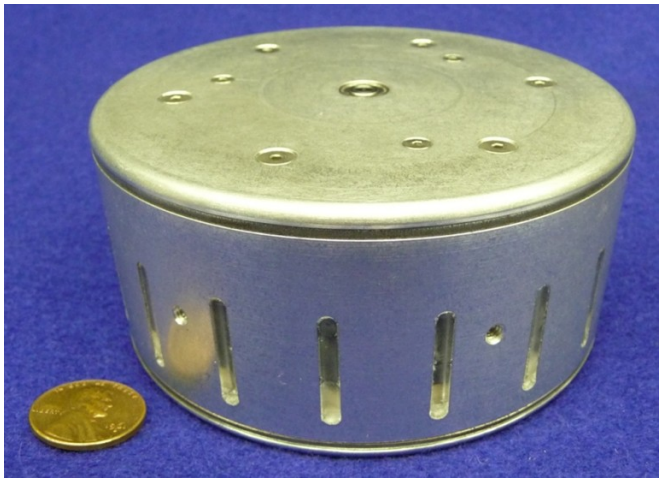

Fig. 4. Fully functional wafer disc brake.

B. Design Relationships

One of the primary design objectives for the WDB is to generate a high torque output. As such, the relationships that govern the resistive torque capability are described here. We assume that the compressive force applied to the annular discs is evenly distributed, and thus that the compressive force results in a constant pressure applied across the annular area of the disc:

$$F = \pi P(r_o^2 - r_i^2) \qquad (1)$$

where F is the compressive force, P is the pressure between discs, and r_i and r_o are the inner and outer radii of the discs, respectively. Assuming Coulomb friction between the discs, the resistive torque generated by the one disc interface is given by:

$$T = \int_{r_i}^{r_o} r\mu P(2\pi r dr) = \frac{2\pi\mu P}{3}(r_o^3 - r_i^3) \qquad (2)$$

where T is the resistive torque and μ is the coefficient of friction (either static or dynamic, depending on whether or not the discs are moving relative to each other). Combining (1) and (2), and assuming a stack of discs, the resistive torque is given as a function of the compressive force by:

$$T = \frac{2\mu FN}{3}\frac{(r_o^3 - r_i^3)}{r_o^2 - r_i^2} \qquad (3)$$

where N is the number of disc interfaces (i.e., between stator and rotor). Assuming that torque is proportional to current in the DC motor, and neglecting friction in the ball screw, the resistive torque can be written as a function of motor current as:

$$T = \frac{2\mu N k_t}{3l}\frac{(r_o^3 - r_i^3)}{r_o^2 - r_i^2} i \qquad (4)$$

where l is the ball screw lead, k_t is the motor torque constant, and i is the motor current. Note that, in the case of a return spring (see Fig. 2), the resistive torque is somewhat less than that described by (4), since the compressive force F is decreased by the spring stiffness. As indicated by (4), maximizing the resistive torque requires maximizing both the output and input radii (e.g., a narrow ring will provide more torque than a wide ring, provided they have the same outer radius). Thus, a tradeoff becomes apparent between maximizing torque and maximizing surface area (which minimizes disc wear). However, the significant benefit of this dimensional phenomenon for this application is that rings may be used instead of solid discs. This fact combined with the design of the brake such that the outer barrel serves as the rotating body (i.e., does not require a central shaft) allows all of the actuation and transmission components to be located concentrically within the disc stack, enhancing compactness of the design. The compression ring was designed with the aid of a finite element analysis of stress such that it was lightweight, while still maintaining sufficient strength to reliably transmit the forces from the ball screw to the disc stack. For a more detailed treatment of torque estimation from annular contact disc brakes and clutches, see [24].

Several of the design variables were inherent to such components as the DC motor and ball screw, which were chosen based on commercial availability and their ability to maximize torque while remaining within an acceptable package size. A 30 W Maxon EC45 DC brushless flat motor was chosen to actuate the brake due to its thin profile and high torque. Importantly, the lack of a gearhead and the use of a ball screw instead of a lead screw allow the motor to remain fully back-drivable. As such, the brake is able to return to either its normally unlocked or normally locked state when the electrical power input is turned off (i.e., when the brake is powered down). A Faulhaber Microlinea ED513 ball screw was chosen based on its small lead (1.25 mm) and low profile ball nut design.

Selection of disc material and disc thickness was accomplished by a finite element analysis of disc stress and iterative testing of several different candidate materials. Key factors in material selection were high tensile strength, high coefficient of friction, and the ability to remain flat after fabrication. While a variety of materials have been shown to work effectively in the brake, including stainless steel, polyetherimide (Ultem), and polyetheretherketone (PEEK), the material chosen based on weight and performance for the brake characterization was wear resistant G-10 phenolic. This ultra high strength glass-epoxy laminate exhibits high dimensional stability over temperature, provides a relatively high coefficient of friction, and is treated to resist wear. The disc thickness was chosen to be 0.25 mm (0.010 in), which provided sufficient rigidity to resist buckling near the spline interfaces, which was found to be the primary mode of failure in thinner discs. The splines themselves were designed as keys inserted into keyways for ease of manufacturing. As an added benefit, this allowed flexibility in the selection of the materials used for the keys. In the design shown in Fig. 4, Ultem was chosen for the key material, which has a high tensile strength, a high maximum operating temperature, and an appropriate hardness to interface with the G-10. The geometrical configuration of the brake prototype, along with the values for the other design parameters given in (4), is given in Table 1. For the normally unlocked configuration, a return spring of stiffness k=3.35 N/mm was utilized, which deflects approximately 13 mm before the pressure plate contacts the disc stack, and thus the compressive force provided by the motor is decreased by approximately 44 N. Accounting for the force required to compress the spring, (4) indicates a predicted maximum static and dynamic torque of the wafer disc brake in the normally unlocked configuration of 83.1 N-m and 54.8 N-m, respectively.

C. Special Considerations for the Normally Locked Design

While operating in the normally locked configuration, the motor acts to release rather than impose compressive force on the disc stack, which essentially decreases rather than increases the resistive torque. In this case, a set of compression springs provides the compressive force on the disc stack. To release the brake, the electric motor must

TABLE I
RESULTS OF THE ANALYTICAL AND EXPERIMENTAL DESIGN OPTIMIZATION

Design Variable	Value
k_t	25.5 mN-m/A
i_{max}	2.14 A
l	1.25 mm
μ_s	0.194
μ_k	0.128
N	44
r_i	39.4 mm
r_o	44.9 mm

provide (through the ball screw) enough force to match the compressive force of the springs on the stack, and additionally to compress the springs another approximately 3mm (i.e., the disc stack is not perfectly flat, and expands slightly when the compressive force is relieved). The maximum force applied to the stack by the springs must therefore be less than the maximum force applied by the motor and ball screw in the normally unlocked case, so that the brake can be fully unlocked. To minimize the amount of motor torque required for disc expansion, the brake design maximizes the linear space available to the springs such that the longest springs possible can be employed. Taking this approach allows the spring constant to be minimized (for a given nominal stack force) which reduces the rate of increase of force as the springs are being compressed. Based on the parameters listed in Table I, the motor and ball screw transmission can generate a maximum force of 274 N. The springs selected for the normally locked brake have a spring constant of 3.2 N/mm, and as such a compression of 3 mm (i.e., to fully relieve the disc stack) requires a force of approximately 10 N. Thus, the normally locked brake can apply a maximum of 264 N to the disc stack in the unpowered state, which is approximately 3.5% less than that of the normally unlocked brake at maximum power. Thus, the maximum static and dynamic torque for the normally locked brake in the unpowered state is predicted to be 80.2 N-m and 52.9 N-m, respectively.

III. BRAKE CONTROL

Based on the idealized steady-state relationship described by (4), control of the current in the brushless motor would also provide control of the steady-state resistive brake torque. Despite this, the dynamic relationship between motor current and resistive brake torque is more complex, and includes the inertial effects of the ball screw and motor rotor, Coulomb friction in the transmission, and stiffness of the return spring and disc stack. The latter two physical effects constitute non-smooth nonlinearities, which complicate the open-loop control of brake torque. The non-smooth nature of Coulomb friction is evident. The non-smooth nature of the "load" stiffness is due to the fact that the discs are not perfectly flat, and as such, three distinct load stiffnesses are present. Prior to contact with the discs, the load stiffness consists only of the return spring; once contact is made with the discs, the load stiffness is the combined effect of the return spring and the compliance of the non-flat discs; finally, once all discs are flattened by the compressive force of the motor/ball screw, the load stiffness increases considerably (i.e., the stiffness is essentially that of the "solid" annular disc stack). The load stiffness therefore can be modeled as piecewise linear stiffness consisting of three regimes: the non-contact regime (return spring only), the flattening regime, and the solid stack regime. As a result of these non-smooth nonlinearities, open-loop control failed to provide desirable control performance, in terms of accuracy and bandwidth. In order to improve torque tracking, an inner servo control loop was first added around the brushless motor, as shown in Fig. 5(a). This inner loop serves to compensate for the inertial dynamics and Coulomb friction in the transmission. Further, by providing improved output disturbance rejection, the inner loop mitigates the effects of the varying load stiffness on the stability of the closed loop. Note that, since the brushless motor incorporates Hall effect sensing for electronic commutation, implementation of the inner loop did not require the addition of any sensors. With the inner loop in place, accurate and robust tracking of the pressure plate motion is provided. However, due to the aforementioned tripartite stiffness, control of pressure plate motion does not provide known control of the compressive force. If the relationship between pressure plate motion and the compressive force were well characterized, the force could be controlled in an open-loop manner. However, there would still exist a significant nonlinearity between the compressive force and the resistive torque, due to the nonlinear friction characteristics in the discs. As such, a resistive torque control outer loop was implemented around brake output torque, as shown in Fig. 5(b). Note that the implementation of the outer loop does require brake torque sensing. As shown subsequently, however, accurate and high bandwidth control of magnetic particle brake also requires a similar closed loop around the brake torque.

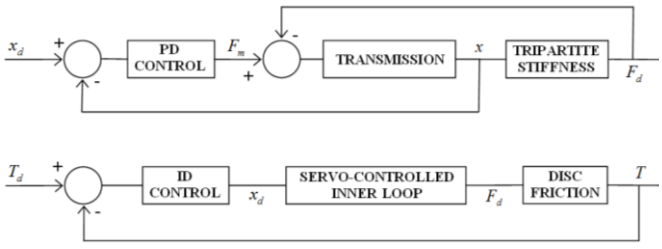

Fig. 5. Schematic of wafer disc brake controller. (a) Servo control inner loop. (b) Torque control outer loop.

IV. Performance Characterization

The wafer disc brake was tested in both operational configurations (normally unlocked and normally locked). The experimental setup used to test the brake torque is shown in Fig. 6. The brake barrel was driven at a constant rate with a DC motor (Kollmorgen model U12M4H) which was connected to the brake through a 90:1 transmission, in order to generate sufficient torque to drive the brake. Note that resistive torque can only be measured when the brake shaft is moving. An encoder attached to the motor provided for closed-loop feedback control of motor velocity, so that velocity remained essentially constant, despite variation in brake torque. Brake torque was measured with a rotary torque transducer (Interface model T8 ECO) mounted between the motor and brake.

Figure 7 shows the maximum and minimum (low-end) dynamic (i.e., when the brake shaft is rotating) steady-state torques of the WDB, measured at a rotational speed of 20 rev/min (RPM). The average maximum torque of the brake was 30 N-m (265 in-lbs) with approximately 5% torque ripple. This maximum torque was lower than that predicted in Section II (i.e., approximately 55% of that predicted by the equations). However, torque values up to 40 N-m were achieved during sinusoid tracking trials. This indicates that in addition to the static or dynamic state of the brake rotor, maximum torque is affected by static friction (or stiction) when the ball screw is motionless. Thus, for the normally unlocked brake, the maximum average dynamic friction was 30 N-m when approached quasi-statically and 40 N-m when approached dynamically. The maximum static torque of the normally unlocked brake was 73 N-m. These values show better agreement with the expected values of 55 N-m and 83 N-m and the remaining difference may be attributed largely to uncertainty in the values for static and dynamic coefficient of friction for the G-10 disc material. The average minimum torque was 0.40 N-m (3.5 in-lbs), giving a dynamic range of approximately 1:100. The maximum dynamic torque of the normally locked brake was unable to be measured in either of the two ball screw operational regimes due to insufficiency in the brake dynamometer. That is, both values were greater than 50 N-m, which is the maximum torque the experimental setup could measure under continuous rotation. The static torque was determined (as was the case for the normally unlocked brake) by providing manual assistance to increase the dynamometer torque to the brake and was measured at 74 N-m. As discussed previously, the normally locked brake torque was predicted to be slightly lower than that of the normally unlocked brake. This deviation from the predicted results is likely also explained by the ball screw friction exhibited between static and dynamic performance.

Figure 8 shows sinusoid tracking capabilities of the normally unlocked brake for a peak-to-peak amplitude of 20 N-m, which is 50% of its full dynamic range. Figure 9 shows rising and falling step responses for the normally locked configuration, also with a 20 N-m amplitude. Defining rise time as the amount of time required after a step

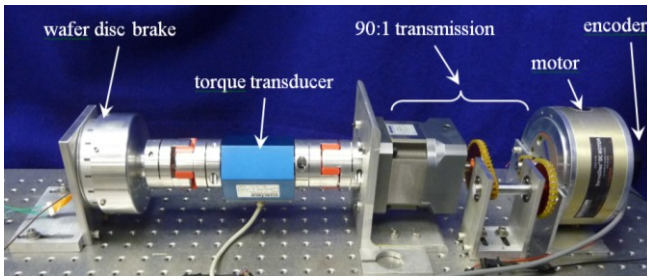

Fig. 6. Experimental setup for testing of the wafer disc brake. Note that, since the output of the WDB is a barrel rather than a shaft, the brake is connected to the setup through an adapter, which transmits torque from the barrel to a central shaft.

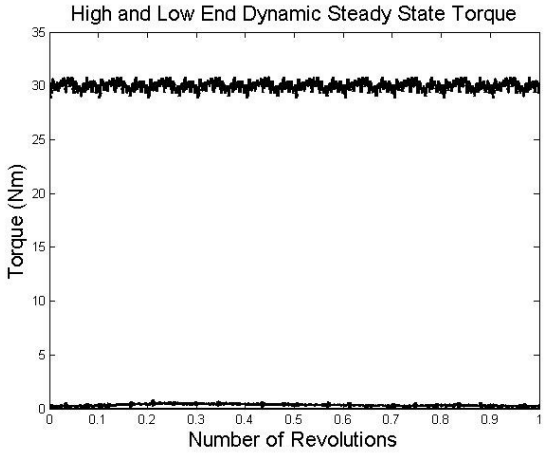

Fig. 7. Maximum and minimum dynamic wafer disc brake torque in normally unlocked configuration for one revolution at a speed of 20 rev/min.

command has been issued for the response to rise to 90% of the final steady-state step value, and the fall time as the reverse, the wafer disc brake demonstrates a rise time of 43 msec and a fall time of 39 msec in the normally unlocked configuration and 53 msec and 39 msec, respectively, in the normally locked configuration. Plots of sinusoid tracking and step response are not provided for the normally locked brake, due to the fact that they appear nearly identical. Bandwidth plots for sinusoidal tracking of 20 N-m peak-to-peak commands are provided for each brake configuration in Figs. 10 and 11, which indicate a -3 dB bandwidth of 11 Hz in the normally unlocked case and 10 Hz in the normally locked case.

An experiment was conducted to determine the power dissipation capacity of the wafer disc brake, the results of which are shown in Fig. 12. A thermocouple was connected inside the body of the brake to monitor the temperature. The brake speed and torque were incrementally increased and held for five minutes at a given power level before the brake temperature was recorded. Due to limitations in power generation from the dynamometer (Fig. 6), data could only be gathered for power dissipation up to 55 W (see Fig. 12). As such, based on this data, the temperature for increasing power dissipation was projected (using the quadratic trend indicated in the data). Based on these projections, power dissipation of 125 W would produce an internal brake temperature of 120 C (250 F), which is the maximum

operating temperature of the brushless DC motor. It should be noted, however, that the design presented herein was not designed to maximize power dissipation, and as such, it be expected that some minor modifications (such as adding vents to the brake body) would result in improved capability for power dissipation.

An experiment was also conducted to determine the rate of wear of the discs. Specifically, the brake was run at a constant speed and torque over a given length of time, and the height (or thickness) of the disc stack was measured both before and after the experiment. The energy dissipation was measured by the dynamometer (based on shaft torque, speed, and duration of the experiment). Based on these measurements, the rate of wear of the discs was determined to be 3.7 microns per kJ of energy dissipation. Based on the dimensions of the brake and the length of travel along the ball screw, the disc stack could tolerate approximately 1.5 mm of wear before performance would begin to degrade. For the case of G-10 discs, this equates to approximately 400 kJ of energy dissipation. If wear is of particular concern for a specific application, other disc materials could be chosen. For example, replacing the G-10 discs with a set of stainless steel discs would presumably provide greatly increased wear resistance, but would increase the brake weight from 0.67 kg to 0.81 kg.

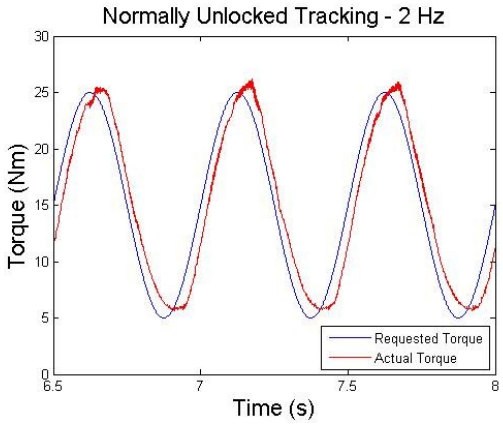

Fig. 8. Normally unlocked brake sinusoid tracking with a peak-to-peak amplitude of 20 N-m (50% of full dynamic range).

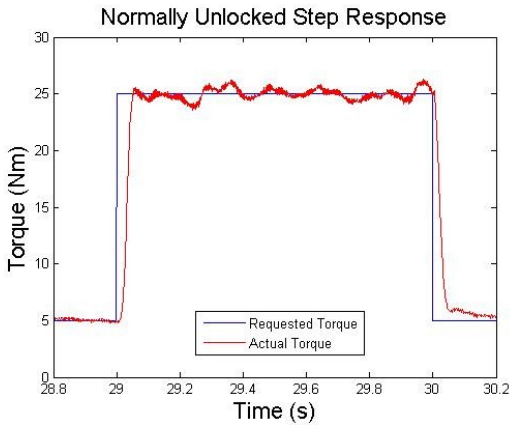

Fig. 9. Normally unlocked brake rising and falling step response with an amplitude of 20 N-m (50% of full dynamic range).

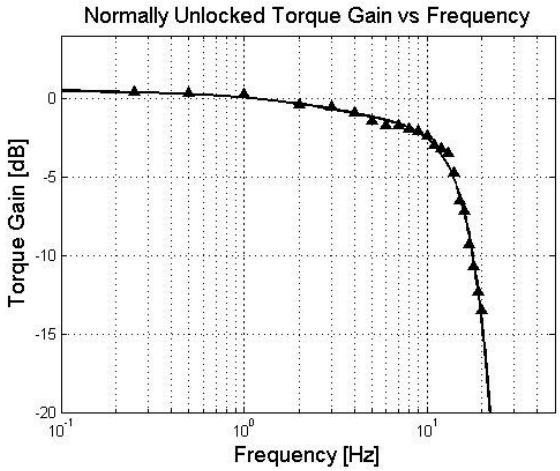

Fig. 10. Normally unlocked torque gain vs. frequency for 20 N-m peak-to-peak oscillations (50% of full dynamic range) indicating a bandwidth of 11 Hz.

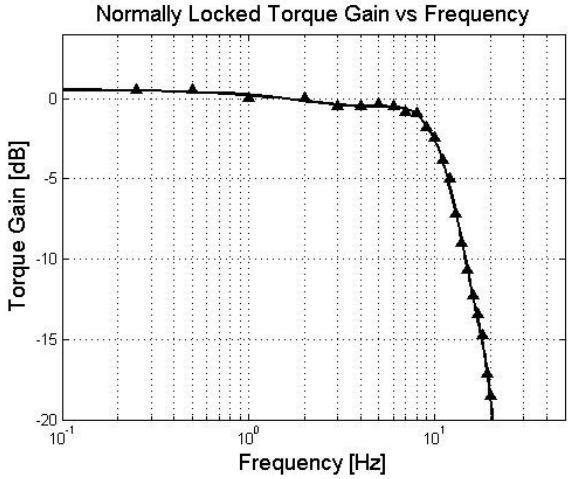

Fig. 11. Normally locked torque gain vs. frequency for 20 N-m peak-to-peak oscillations (50% of full dynamic range) indicating a bandwidth of 10 Hz.

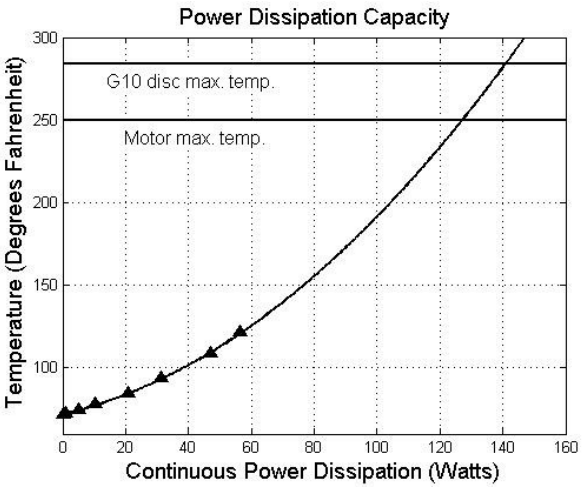

Fig. 12. Wafer disc brake power dissipation capacity based on maximum permissible temperature, predicting a maximum power dissipation level of 125 W.

TABLE II
COMPARISON OF THE B115 MAGNETIC PARTICLE BRAKE WITH THE WAFER DISC BRAKE

Characteristic	B115 MPB	Normally Unlocked WDB	Normally Locked WDB
Max Dynamic Torque [N-m](in-lbs.)	13.0 (115)	40 (354)	50+ (443+)
Max Static Torque [N-m](in-lbs.)	16.6 (147)	73 (646)	74 (655)
Min Torque [N-m](in-lbs.)	0.28 (2.5)	0.40 (3.5)	0.40 (3.5)
Torque Ripple [%], Open Loop Control	2.7	-	-
Dynamic Torque-to-Weight [N-m/kg]	3.58	59.7	74.6+
Dynamic Range	1:46	1:100	1:125+
Rise Time [s], Open Loop Control Closed Loop Control	0.420 0.043	- 0.043	- 0.053
Bandwidth for ± 25% FS Oscillations [Hz] Open Loop Control Closed Loop Control	 2 22	 - 11	 - 10
Steady-State Power Consumption (Normalized by torque) [W/N-m]	0.87	0.26	0.22
Max Continuous Power Dissipation [W]	55	125	125
Weight [kg](lbs.)	3.63 (8.0)	0.67 (1.48)	0.67 (1.48)
Diameter [mm](in)	120 (4.71)	102 (4.00)	102 (4.00)
Length [mm](in)	66.8 (2.63)	47.6 (1.88)	47.6 (1.88)

V. COMPARISON OF WAFER DISC BRAKE AND MAGNETIC PARTICLE BRAKE

To place the performance of the wafer disc brake in context, the performance characteristics were compared with those of a commercially available magnetic particle brake of comparable size. The particle brake utilized for the comparison was a Placid Industries model B115, which measures approximately 12.0 cm in diameter by 6.7 cm in length, as compared with the wafer disc brake which measures 10.2 cm in diameter and 4.8 cm in length. While possessing a similar size, it should be noted that the MPB has a mass of over five times that of the wafer disc brake, weighing 3.63 kg compared to 0.67 kg for the wafer disc brake.

The most obvious advantage of the wafer disc brake is the high torque capability relative to its weight. The 0.67 kg WDB provides a maximum dynamic torque of 40 N-m while the 3.63 kg MPB only provides 13 N-m. This gives the WDB a dynamic torque-to-weight ratio of about 60 compared to that of the MPB which is about 3.6. Thus, the wafer disc brake offers a torque-to-weight ratio of over 17 times that of a comparably sized magnetic particle brake. Additionally the WDB also provides a greater dynamic range, specifically 1:100 compared to the MPB's dynamic range of 1:46.

Figure 13 shows the step responses of both the wafer disc brake and the magnetic particle brake. Both operational modes of the WDB are represented and both control modes (open and closed-loop) of the MPB are represented. The rise times of the normally unlocked and normally locked brake (as previously presented) are 43 and 53 msec, respectively. The open-loop controlled MPB rise time is 420 msec, and the closed-loop MPB rise time is 43 msec. It should be noted, however, that the WDB step represents 20 N-m, while the MPB step represents 6.5 N-m of torque (i.e., both were characterized at 50% of their respective ranges). Thus, the WDB exhibits similar response speed to the MPB, but would be significantly faster if characterized in terms of a torque slew rate. The bandwidth of the MPB for tracking of steady-state sinusoidal commands (of 50% full scale torque) is 2 Hz and 22 Hz, respectively, for the open-loop and closed-loop controlled MPB. Thus, while the rise times of the WDB are faster in all cases, the closed-loop controlled MPB demonstrates a somewhat higher bandwidth than the closed-loop controlled WDB (although both are on the same order).

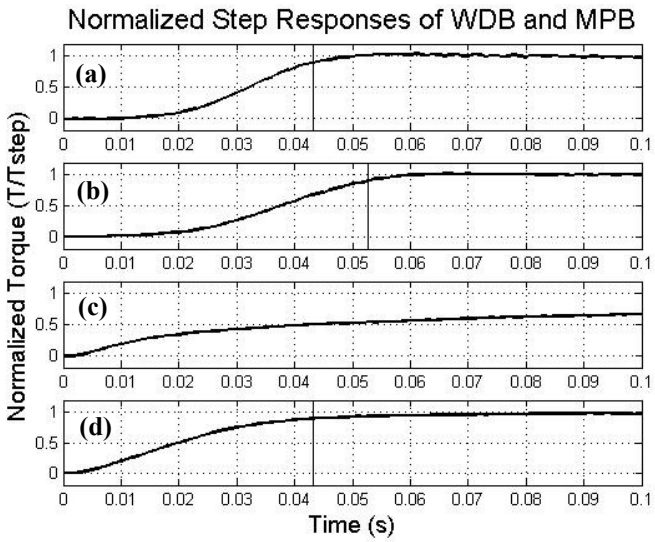

Fig. 13. Normalized step responses of wafer disc brake and magnetic particle brake with step command initiation at time = 0 seconds. (a) Normally unlocked brake response (Tstep = 20 N-m). (b) Normally locked brake response (Tstep = 20 N-m). (c) Particle brake response in open-loop (Tstep = 6.5 N-m). (d) Particle brake response in closed-loop (Tstep = 6.5 N-m).

As mentioned previously, a potential advantage of the WDB is a reduction in electrical power consumption for a given resistive torque. The steady-state power consumption for the WDB normalized by output resistive torque is 0.26 and 0.22 W/N-m for the normally unlocked and normally locked brakes, respectively. The MPB requires 0.87 W/N-m, and thus the WDB requires approximately one third the electrical power of the MPB for a given output resistive torque. Further, as previously stated, the normally locked version of the WDB may save additional power in cases that require greater than 50% duty cycle of resistive torque.

Finally, in comparing the torque ripple of both devices, the open-loop and closed-loop controlled MPB exhibits 2.7% and 1.5%, respectively, while the WDB (as previously mentioned) exhibits a torque ripple of approximately 5%. Table 2 summarizes the performance characteristics of the wafer disc brake versus those of the magnetic particle brake.

VI. Conclusion and Recommendations

The authors have presented a design for an electrically actuated proportional brake, called a wafer disc brake (WDB), that offers some significant advances relative to a magnetic particle brake (MPB, considered the benchmark of such devices). Specifically, the WDB exhibits a torque-to-weight ratio that is more than an order of magnitude larger than the MPB, while requiring less than one third of the steady-state electrical power for a given level of resistive torque. Further, the unlike the MPB and most other previously reported devices, the WDB can be configured in a normally unlocked or normally locked configuration.

Despite significant advantages, the WDB also has some disadvantages relative to an MPB. One potential disadvantage of the WDB is disc wear, although this could be mitigated with the use of more wear-resistant discs (such as stainless steel or ceramic). The WDB also exhibits somewhat greater torque ripple relative to the MPB. As discussed herein, control of the WDB is more complex than control of the MPB, although accurate torque tracking and good dynamic performance requires an outer torque loop for both. Finally, as currently designed, the WDB is likely more expensive to produce that a MPB.

References

[1] R. J. Farris, Hugo A. Quintero, Thomas J. Withrow, and Michael Goldfarb, "Design and Simulation of a Joint-Coupled Orthosis for Regulating FES-Aided Gait" *Robotics and Automation, 2009 IEEE International Conference on* , pp.1916-1922, May 2009.

[2] R. J. Farris, Hugo A. Quintero, Thomas J. Withrow, and Michael Goldfarb, "Design of a Joint-Coupled Orthosis for FES-Aided Gait" *Rehabilitation Robotics, 2009 IEEE International Conference on* , pp.246-252, April 2009.

[3] M. Goldfarb, W. Durfee, K. Korkowski, and B. Harrold. Evaluation of a Controlled-Brake Orthosis for FES-Aided Gait, IEEE Transactions on Neural Systems and Rehabilitative Engineering, vol. 11, no. 3, pp. 241-248, 2003.

[4] M. Goldfarb and W. Durfee. Design of a Controlled-Brake Orthosis for Regulating FES-Aided Gait. IEEE Transactions on Rehabilitation Engineering, vol. 4, no. 1, pp. 13-24, 1996.

[5] B. Weinberg et al., "Design, Control and Human Testing of an Active Knee Rehabilitation Orthotic Device," Robotics and Automation, 2007 IEEE International Conference on , pp.4126-4133, 10-14 April 2007

[6] J. Chen and W. Liao, "Design and control of a Magnetorheological actuator for leg exoskeleton," Robotics and Biomimetics, 2007. ROBIO 2007. IEEE International Conference on , pp.1388-1393, Dec. 2007

[7] B. Aeyels, W. Van Petegem, J. Vander Sloten, G. Van der Perre, and L. Peeraer, "EMG-based finite state approach for a microcomputer-controlled above-knee prosthesis," Proceedings for the IEEE Engineering in Medicine and Biology 17th Annual Conference, vol. 17, no. 2, pp. 1315-1316, Sep. 1995.

[8] W. S. Harwin, L. O. Leiber, G. P. G. Austwick, and C. Dislis, "Clinical potential and design of programmable mechanical impedances for orthotic applications," Robotica, vol.16, pp. 523-530, Sep.-Oct. 1998.

[9] H. Herr, and A. Wilkenfeld, "User-Adaptive Control of a Magnetorheological Prosthetic Knee," Industrial Robot: An International Journal. 2003; 30: 42-55.

[10] J. Furusho et al., "Development of Shear Type Compact MR Brake for the Intelligent Ankle-Foot Orthosis and Its Control; Research and Development in NEDO for Practical Application of Human Support Robot," Rehabilitation Robotics, 2007. ICORR 2007. IEEE 10th International Conference on , pp.89-94, June 2007

[11] Changhyun Cho; Jae-Bok Song; Munsang Kim, "Energy-Based Control of a Haptic Device Using Brakes," Systems, Man, and Cybernetics, Part B: Cybernetics, IEEE Transactions on, vol.37, no.2, pp.341-349, April 2007

[12] Jinung An; Dong-soo Kwon, "Haptic experimentation on a hybrid active/passive force feedback device," Robotics and Automation, 2002. Proceedings. ICRA '02. IEEE International Conference on , vol.4, pp. 4217-4222, 2002

[13] Ying Jin; Furusho, J.; Kikuchi, T.; Oda, K.; Takashima, S., "A basic study on passive force display and rehabilitation system with redundant brakes," Complex Medical Engineering, 2009. CME. ICME International Conference on , pp.1-6, 9-11 April 2009

[14] M. Sakaguchi, et al., "Passive force display using ER brakes and its control experiments," Virtual Reality, 2001. Proceedings. IEEE , pp.7-12, 17-17 March 2001

[15] ZhiDong Wang; Fukaya, K.; Hirata, Y.; Kosuge, K., "Control Passive Mobile Robots for Object Transportation - Braking Torque Analysis and Motion Control," Robotics and Automation, 2007 IEEE International Conference on , pp.2874-2879, 10-14 April 2007.

[16] N.M. Mayer, F. Farkas, and M. Asada, "Balanced walking and rapid movements in a biped robot by using a symmetric rotor and a brake," Mechatronics and Automation, 2005 IEEE International Conference , vol.1, pp. 345-350, 29 July-1 Aug. 2005.

[17] Ahn Kyoung Kwan; Tran Hai Nam; Yoon Young Il, "New approach to design MR brake using a small steel roller as a large size magnetic particle," Control, Automation and Systems, 2008. ICCAS 2008. International Conference on , pp.2640-2644, 14-17 Oct. 2008.

[18] B. Kavlicoglu, F. Gordaninejad, and C. Evrensel, "A Semi-Active, High-Torque, Magnetorheological Fluid Limited Slip Differential Clutch," Journal of Vibration and Acoustics, vol.128, issue5, pp.604-611, Oct. 2006.

[19] K. Karakoc, E. J. Park, and A. Suleman, Design considerations for an automotive magnetorheological brake, Mechatronics, vol.18, issue8, Pages 434-447, Oct. 2008.

[20] W.H. Li, and H. Du, "Design and Experimental Evaluation of a Magnetorheological Brake," The International Journal of Advanced Manufacturing Technology, vol.21, issue7, pp.508-515, May 2003.

[21] Gosline, and V. Hayward, "Eddy Current Brakes for Haptic Interfaces: Design, Identification, and Control," Mechatronics, IEEE/ASME Transactions on , vol.13, no.6, pp.669-677, Dec. 2008.

[22] D. Senkal, and H. Gurocak, "Compact MR-brake with serpentine flux path for haptics applications," EuroHaptics conference, 2009 and Symposium on Haptic Interfaces for Virtual Environment and Teleoperator Systems. World Haptics 2009. Third Joint , pp.91-96, 18-20 March 2009.

[23] M. Gogola, and M. Goldfarb, "Design of a PZT-actuated proportional drum brake," Mechatronics, IEEE/ASME Transactions on , vol.4, no.4, pp.409-416, Dec 1999.

[24] W. C. Orthwein, Clutches and Brakes Design and Selection, Second Ed., Chapter 5, Carbondale, IL, Marcel Dekker, Inc., 2004.